

The Impact of Cooling Rate on the Tensile and Cyclic Stress-strain Characteristics of Different Solder Alloys at Nanoscale

Sadib Fardin, Md. Jawarul Moresalein, Toushiqul Islam, Abrar Faiyad and Mohammad Motalab*

Department of Mechanical Engineering, Bangladesh University of Engineering and Technology, Dhaka - 1000, Bangladesh

sadib.fardin@gmail.com, moresaleinayon1998@gmail.com, toushiqul.islam03@gmail.com, afaiyad@ucmerced.com, abdulmotalab@me.buet.ac.bd (*corresponding author)

ABSTRACT

In recent years, lead-free solder alloys, such as those based on tin, silver, or copper, have acquired popularity over lead-based solder alloys due to their improved mechanical and electrical properties, coupled with their non-toxic nature. In our previous studies, the stress-strain behavior of SAC305 was studied under varying cooling rate. This study investigates various lead-free solder materials such as Sn, Sn-Ag, and SAC305 to compare the relative mechanical and cyclic properties of lead-free solder materials. The cooling rate is an important controlling parameter of microstructure and mechanical properties and hence, by using molecular dynamics, the atomistic models are first melted at a constant rate and then cooled at various rates, including 2.5 K/ps, 10 K/ps, 50 K/ps, and 100 K/ps. Additionally, an exponential cooling is also used to resemble real-world cooling phenomena like air cooling, water cooling, and furnace cooling. A set of modified embedded atomic model (MEAM) interatomic potentials are used to perform the tensile test and cyclic loading. The tensile test has been conducted until fracture occurred at a strain rate of $1 \times 10^9 \text{ s}^{-1}$. In addition, the cyclic loading behavior of the materials in the strain range of -10% to 10% for 10 cycles are investigated. The result implies that cooling rates have a substantial influence on mechanical properties, with slower cooling rates (2.5 K/ps and 10 K/ps) having a considerable difference and between the higher cooling rates (50 K/ps and 100 K/ps) the observed alterations in mechanical properties are not substantial. The ultimate strength, Young's modulus, modulus of resilience, and coefficient of thermal expansion are negatively correlated with increasing cooling rates. The modulus of toughness exhibits an increasing trend, indicating that the capacity to resist impact loading has increased. To comprehend the extent of energy dissipation during cyclic loading, the hysteresis loop area and stress amplitude of cyclic loading have been examined. After

a certain number of cycles, the amount of energy lost during each cycle stops increasing and stabilizes.

Keywords: Molecular Dynamics Simulations, Lead-Free Solder, Solidification, Tensile and Cyclic Behavior.

NOMENCLATURE

E	Total energy
F	Embedding energy
m	Mass
P	Pressure
r	Interatomic distance
T	Temperature
v	Velocity
<i>Greek symbols</i>	
ρ	Atomic electron density
ϕ	Pair potential interaction
σ	Stress
τ	Time constant
ϵ	Strain
Ω	Atomic volume
<i>Superscript</i>	
α, β	Atomic indices
<i>Subscript</i>	
i, j	Indices in Cartesian coordinate system
<i>Abbreviations</i>	
CTE	Coefficient of thermal expansion
UTS	Ultimate tensile strength
YM	Young's modulus

1. INTRODUCTION

The electronics industry is moving toward lead-free soldering technique because of environmental and health concerns [1]. To replace lead, numerous lead-free materials were created, including Sn, Sn-Ag, and Sn-Ag-Cu (SAC), and their mechanical and thermal properties were examined to ensure their dependability [2-4]. Lead-free solder materials possess exceptional properties such as a lower melting point [5], excellent wetting and solderability [6], improved thermal and mechanical properties [7, 8], compatibility with common electronic components [9, 10], and relatively high electrical conductivity [11]. As a result, they have crucial applications in solder bumping for flip chip connections, die bonding, mounting microelectronic devices, surface mount technology (SMT), and plated-through-hole (PTH) assembly techniques [12-14]. However, despite these advantages, there are persistent issues such as dissolution of Cu, excessive intermetallic compounds, relatively high cost and tin whiskers [15-17]. Sn-Pb is popular due to its lower melting point, lowered surface tension, and ability to inhibit the change of white tin to grey by acting as a solvent element [18].

The tensile properties of lead based and lead-free are compared in terms of different temperature and strain rate [19]. The issue of fatigue loading holds significant importance in Micro-electromechanical systems (MEMS) applications over their operational lifespan [20]. Pang et al. [21] studied the temperature and strain rate on the fatigue life of solder joint by finite element method. Lall et al. [22] investigates the characterization of SAC solder after extended storage at low temperatures and high strain rates to determine nine anand parameters from tensile data. Chowdhury et al. [23] used water quenched solidification profile to analyze the mechanical properties of doped SAC solder materials. Basaran et al. [24] investigated the material response to concurrent vibration and thermal loading. Wiese et al. [25] used cyclic triangular strain wave to examine the durability of solder materials in different applications. Fatigue life of SAC and Sn-Pb has been compared for different package type by Schubert et al. [26].

Several numerical studies of lead-free solder material have been conducted in recent years. SAC alloy with varying Ag content at different temperature to evaluate the thermomechanical properties computationally [27]. Zhang et al. [28] studied the tin whiskers growth and IMC evolution of SAC307 by computational method. Zhang et al. [29] utilized numerical simulations to analyze the diffusivity of atoms at the $Ag_3Sn-\beta Sn$ interface in Sn-Ag solder to understand the vital micro-

mechanism for controlling void formation and improving solder joint properties. Shear deformation of Sn based solder joint has been numerically and experimentally investigated by Li et al. [30]. Chen et al. [31] demonstrated cyclic stress-strain of Ni-based single crystal alloy by modulating the temperature, range of strain under cyclic loading. Alvi et al. [32] conducted cyclic and tensile test to study the dislocations and defects of Gold-Silver core shell systems. Nguyen et al. [33] examined temperature and strain rate effects on cyclic plasticity in AlCrCuFeNi HEA and found that interactions between partial dislocations induced lattice disorders during deformation.

The solidification process can be analyzed by different computational processes such as Monte Carlo simulation, finite element simulation, and phase-field simulation [34-36]. The microstructure, which is a key determinant of the mechanical properties, is directly affected by the solidification process [37-39]. Molecular dynamics can be used to observe the microstructure at each step of quenching and understand the solidification process [40]. Recently, Li et al. [41] studied the nucleation process and grain growth of AlCoCrCuFeNi in a wide range of cooling rate. Shen et al. [42] rapidly quenched the Al to examine the glass formation and microstructure. In another study by Li et al. [43], correlated different structure due to varying cooling rate with the strength of tungsten. Shu et al. [44] investigated substructure formation in AlN/FeNiCrCo composite during rapid solidification via selective laser melting, revealing subgrain boundaries and a dense dislocation network arising from heat transfer and lattice mismatches.

To the best of the authors' knowledge, there has been no numerical analysis conducted at the nanoscale level to examine the impact of quenching rates on different solder alloys. In this study, Sn, Sn-Ag, and SAC305 are melted above melting point at a constant cooling rate and then quenched at varying cooling rates such as 2.5 K/ps, 5 K/ps, 50 K/ps and 100 K/ps and an exponential cooling rate. The resulting models after solidification process are subjected to uniaxial tensile and fatigue loading. The investigation of changes in mechanical and thermal properties resulting from various cooling rates in solder alloys are evaluated in terms of ultimate tensile strength (UTS), young's modulus (YM), modulus of toughness and modulus resilience. The models of solder alloys after solidification are also subjected to cyclic loading to analyze the hysteresis loop area per cycle and stress amplitude. The present study utilizes the modified embedded atomic model (MEAM) potential [45, 46].

2. METHODOLOGY

2.1 MEAM POTENTIAL

The present study employs the Large-scale Atomic/Molecular Massively Parallel Simulator (LAMMPS) to execute molecular dynamics simulation, wherein a modified embedded atom method (MEAM) is utilized for interatomic bonding. The MEAM potential has been found to demonstrate greater precision in characterizing intermetallic interactions compared to the EAM potential, due to its inclusion of angular forces. The force field consists of two fundamental energy components, namely the embedding energy potential and the pair potential. As per the MEAM formulation, the sum of the energies of all the atoms in a system, E can be expressed by:

$$E = \sum_i \left\{ F_i(\bar{\rho}_i) + \frac{1}{2} \sum_{i \neq j} \phi_{ij}(r_{ij}) \right\}, \quad (1)$$

Here, the parameter F represents the embedding energy, which is dependent on the electron density of the atom denoted by ρ and pair potential interaction is denoted by ϕ . The summation of the pair potential interaction is conducted over all neighboring atoms j of atom i that are located within a specified cutoff distance.

The relevant literature has previously established and documented the MEAM parameters for binary materials consisting of Sn, Ag, and Cu. Table 1 presents the established parameters corresponding to the solder materials for the current investigation.

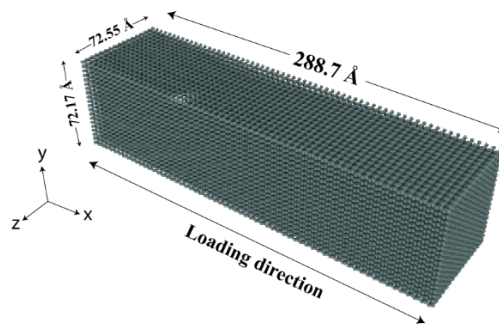
Table 1: MEAM parameters of Sn, Sn-Ag, SAC305 [47-49]

Parameters	Sn	Ag	Cu	Sn-Ag	Ag-Cu	Cu-Sn
E_c (eV)	3.08	2.85	3.54	3.14	3.5	2.8
r_0 (Å)	3.44	2.92	2.54	2.58	2.21	2.36
α	5.09	5.89	5.1	5.8	5.78	5
A	1.12	1.06	1.07			
$\beta(0)$	5.42	4.45	3.63			

$\beta(1)$	8	2.20	2.20
$\beta(2)$	5	6	6
$\beta(3)$	6	2.20	2.20
$t(0)$	1	1	1
$t(1)$	3	5.541	3.138
$t(2)$	5.707	2.45	2.494
$t(3)$	0.3	1.288	2.95

2.2 ATOMIC STRUCTURE MODELING

The present investigation involves the modelling of four distinct nanostructures of different solder alloys, namely Sn, Sn-Ag, and SAC305. The β -Sn atomic model is constructed using AtomsK software within a box having dimensions of 288.7 x 72.17 x 72.55 (Å) as shown in Figure 1 where atoms are colored based on their respective atom type. Then the Sn atoms undergo a random replacement process with Ag, and Cu according to their respective proportions as illustrated in Figure 1. For fatigue tests, the dimension along the x axis is scaled down to a 2:1 ratio, while the dimensions along the y and z axes remain constant. The reduction of aspect ratio is implemented as a measure against the buckling problems that may occur during the compression process. The atomic structures employed for tensile tests consist of 81920 atoms, whereas those utilized for fatigue tests comprise 40960 atoms.



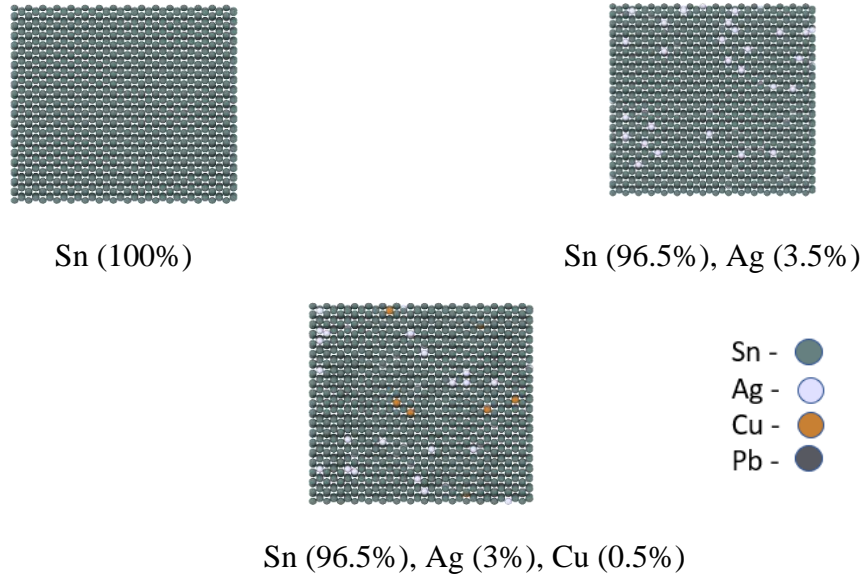


Figure 1: The atomic model of the β -Sn and Illustrations of the three different materials with their proportions.

2.3 MD SIMULATIONS

The molecular dynamics simulations of quenched solder alloys were conducted utilizing the open source software LAMMPS [50], and the resulting data was visualized through the utilization of OVITO [51]. To maintain computational efficiency and accuracy, the time step is fixed at 1 fs. Energy equilibration is performed for 12.5 picoseconds using an NVE ensemble with a Langevin thermostat. The simulations are conducted in the NPT ensemble, utilizing the Langevin thermostat method to retain a constant temperature, T and the Berendsen barostat method to keep a constant pressure, P . The systems are then relaxed in NPT ensemble for 12.5 ps. The temporal variation of temperature during melting and solidification process has been illustrated in Figure 2. To melt the materials, all the systems are heated from 300 K to 1200 K at a constant heat rate of 10 K/ps (A-B). To ensure complete liquification, the system is held at 1200 K for 12.5 ps (B-C). Subsequently, the system is cooled down to 300 K at various cooling rates such as 2.5 K/ps (C-D), 10 K/ps (C-E), 50 K/ps (C-F) and 100 K/ps (C-G). An exponential cooling (C-H) is also employed to resemble the cooling profile found in air cooling, water bath cooling or furnace cooling [52]. In this case, the temperature follows Equation 2 and it is maintained by a loop of NPT ensemble. After quenching, the systems are equilibrated at 300 K. A strain rate of $1 \times 10^9 \text{ s}^{-1}$ is applied to all the samples along the x direction within NVT ensemble until the fracture occurs. To perform cyclic

loading, all the systems are subjected to -10% strain to 10% strain of their initial length to employ some plastic deformation to the solder alloys. The cyclic loading is applied for 10 cycles to study the area under curve in the cycles. The stresses in the structures are calculated using the virial stress theorem [53], following Equation 3.

$$T = 1200e^{-\tau n} \quad (2)$$

$$\sigma_{ij}^{\alpha} = \frac{1}{\Omega^{\alpha}} \left(\frac{1}{2} m^{\alpha} v_i^{\alpha} v_j^{\alpha} + \sum_{\beta=1, n} r_{\alpha\beta}^j f_{\alpha\beta}^i \right) \quad (3)$$

Wherein Equation 2, $\tau = 0.03$ is the time constant of the temperature profile and n is the number of step in the loop. In Equation 3, i and j are the indices in the general Cartesian coordinate system, α and β are the atomic indices, m^{α} and v^{α} denote the mass and velocity of the atom, $r_{\alpha\beta}^j$ is the distance between the atoms α and β , Ω^{α} is the atomic volume of atom α .

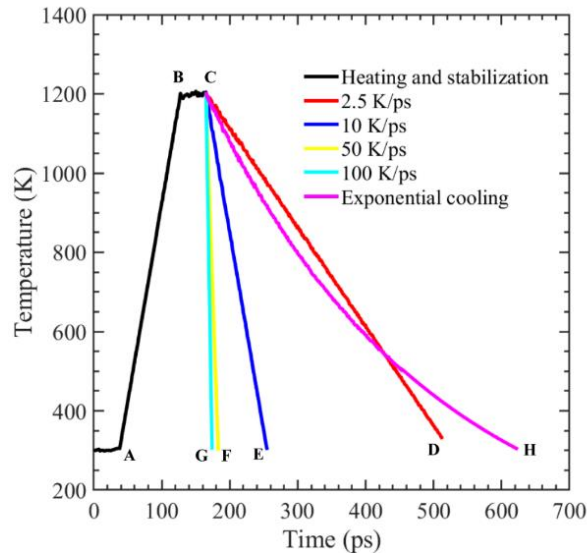


Figure 2: Temperature profile during heating and cooling of the structure.

3. METHOD VALIDATION

In the heating process, the temperature of the system is raised from 300 K to 1200 K, which exceeded the melting point of SAC305. In order to validate the accuracy of our model, the total energy of the system is plotted against the temperature change, as shown in Figure 3, to identify the region of melting. Initially, the model is found in solid phase within region (i). Afterwards, a

significant rise in the slope of the total energy curve is seen between points A and B in region (ii), which signifies the initiation of bond breaking due to a structural phase transition. Furthermore. A distinct change in the slope is visible starting at point B across region (iii), indicating the complete liquefaction of the substance. The initial transition point in the slope was observed at around 490 K, which closely corresponds to the experimental finding of 494 K [54], thereby verifying the accuracy of our model.

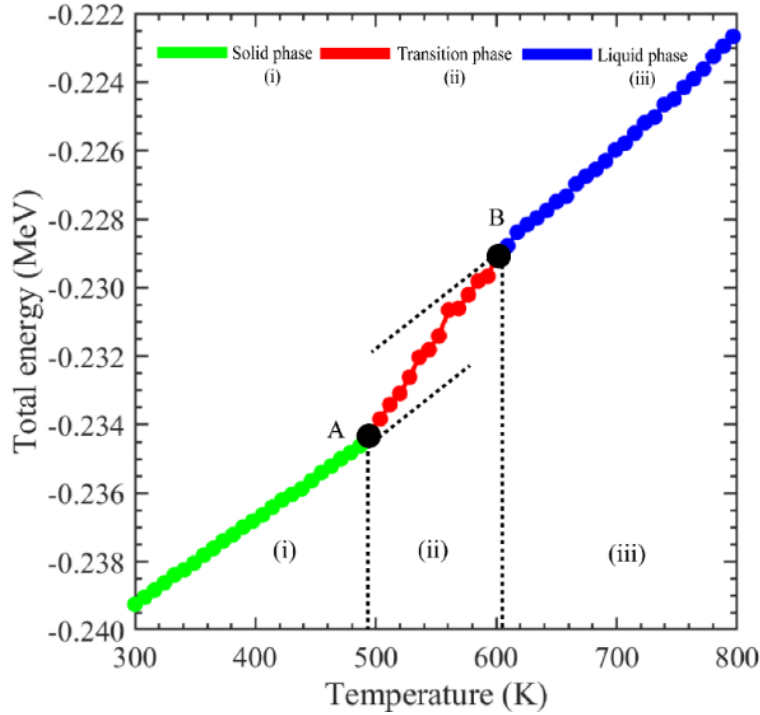


Figure 3: Change in the overall energy of the SAC305 configuration is observed as the temperature is raised.

Notable previous studies' results are listed in Table 2 for validating the computational method that is used in present work.

Table 2: Validation against the experimental studies by CTE

Materials	Previous Experiments (10^{-6} K^{-1})	This Study (10^{-6} K^{-1})
Sn	24-29.5 [55]	23.8
Sn-Ag	19.4-23.2 [56]	25.9
SAC305	17.6-23.6 [56]	22.1

4. RESULTS AND DISCUSSION

4.1 UNIAXIAL TENSILE LOAD

The stress-strain curve of Sn, Sn-Ag, and SAC305 at constant strain rate of $1 \times 10^9 \text{ s}^{-1}$ are plotted in Figure 4 for various cooling rates (2.5 K/ps, 10 K/ps, 50 Kps, 100 K/ps, and exponential cooling). The difference among the stress-strain curves is visible. For higher cooling rates, such as 50 K/ps and 100 K/ps, there is no significant change in stress-strain behavior. When the rate of cooling is increased from 2.5 K/ps to 50 K/ps, the mechanical properties are significantly changed. The exponential cooling curve yields equivalent results to the 2.5 K/ps curve. Elastic deformation occurs around 5-6% strain and then plastic deformation continues.

The changes of UTS and YM in stress-strain curve for all materials at cooling rate of 2.5 K/ps, 10 K/ps, 50 K/ps and 100 K/ps are depicted in Figure 5 and 6. It is observed that an increase in cooling rate reduces the UTS of the lead-free solder alloys. When the cooling rate is raised from 2.5 K/ps to 100 K/ps, the UTS decreases from 6.42 GPa to 5.60 GPa, 6.83 GPa to 6.04 GPa, and 6.90 GPa to 10.91 GPa denoting 12.77%, 11.55%, and 10.91% reduction in case of Sn, Sn-Ag, and SAC305. As the cooling rate is increased from 2.5 K/ps to 100 K/ps, the YM experiences a decrease similar to UTS. For Sn, the YM decreases from 6.42 GPa to 5.60 GPa, representing a reduction of 12.77%. Similarly, for Sn-Ag, the YM decreases from 6.83 GPa to 6.04 GPa, reflecting an 11.55% reduction. In the case of SAC305, the YM decreases from 6.90 GPa to 10.91 GPa, indicating a 10.91% reduction. When the cooling rate is increased, the atoms have less time to arrange themselves and, hence creating defects. This results in degradation in UTS and YM for all lead-free solder alloys. Another notable observation is that both the UTS and YM do not differ much between the case of 50 K/ps and 100 K/ps. This can be explained by changing the microstructure from crystalline to amorphous characteristics of the structure due to rapid solidification process and microstructures do not change considerably. Furthermore, SAC305 has the maximum UTS among all materials, while Sn has the lowest UTS. In the case of YM, SAC305 alloy also exhibits the highest YM, while pure Sn has the lowest YM. The high affinity and the formation of intermetallic compounds of Ag and Cu with Sn lead to the formation of strong bonds with Sn atoms in SAC305 solder [57]. These strong bonds increase the resistance to deformation, resulting in a higher UTS and YM for the SAC305 alloy.

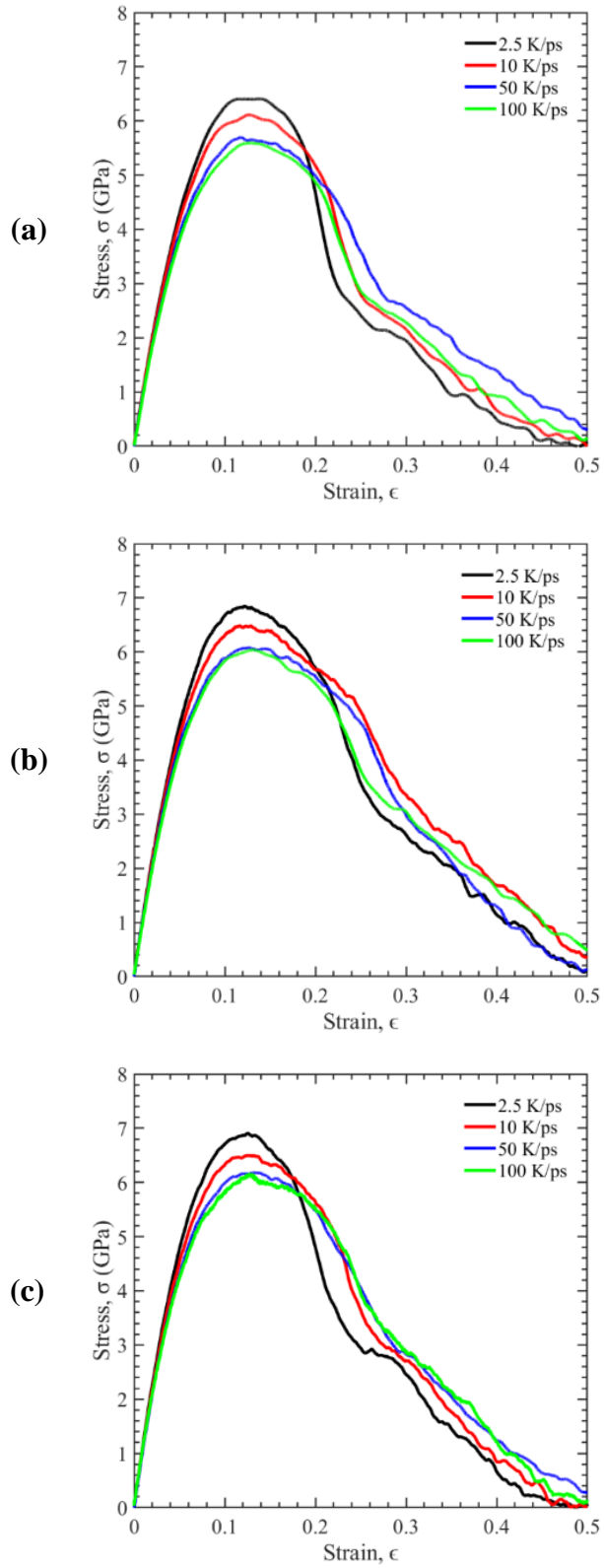


Figure 4: Stress-strain curves for different cooling rates of (a)Sn, (b) Sn-Ag, (c) SAC305

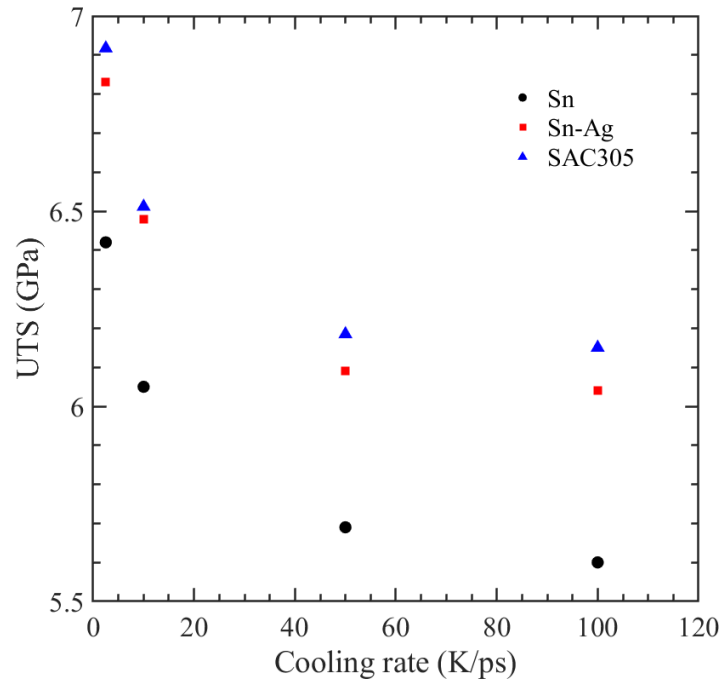


Figure 5: Variation of UTS with cooling rate

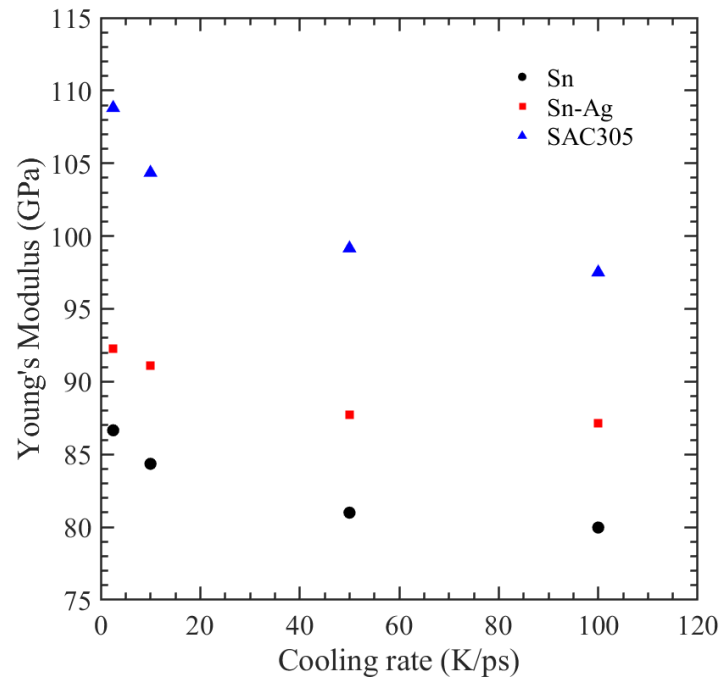


Figure 6: Variation of YM with cooling rate

The area under the curve is calculated to obtain the modulus of toughness and the results are displayed against the cooling rates in Figure 7. Increasing the cooling rate results in an increase in the modulus of toughness, indicating an enhanced capacity to absorb energy. It increases by 10.42%, 10.19%, 6.96% for Sn, Sn-Ag, SAC305, respectively when cooling rate raised from 2.5 to 100 K/ps. As mentioned earlier, the higher density of defects like dislocations and grain boundaries that occur with faster cooling rates can serve as sites for energy dissipation during deformation. Additionally, the formation of intermetallic compounds can contribute to increased toughness by providing additional sites for energy absorption. The addition of Cu to solder materials can potentially decrease their ductility by forming larger and more brittle intermetallic compounds. These intermetallic compounds can act as stress concentration points, making the solder alloy more prone to localized failure by reducing the strain energy absorption capacity of the SAC305 [58, 59]. Thus, among all the materials, Sn-Ag has the highest modulus of toughness indicating more ductile than other materials and Sn has the lowest.

The graph shown in Figure 8 demonstrates the modulus of resilience of all alloys with increasing cooling rates. This parameter characterizes the capacity of a material to absorb and subsequently restore elastic strain energy during elastic deformation. In contrast to the modulus of toughness, the modulus of elasticity decreases with increasing the cooling rate. When the cooling rate is increased from 2.5 K/ps to 100 K/ps, there is a reduction of 10.42% for Sn, 10.19% for Sn-Ag, and 6.96% for SAC305. It suggests that the ability of material to absorb and store elastic energy is decreasing with cooling rates. By incorporating Ag and Cu into the composition, the strength of solder alloys is increased, resulting in SAC305 having the highest modulus of resilience and pure Sn having the lowest modulus of resilience among all materials and cooling rates. Both modulus of toughness and modulus of resilience for 50 K/ps and 100 K/ps are almost similar which further employs the amorphous structure at higher cooling rate (50 K/ps and 100 K/ps)

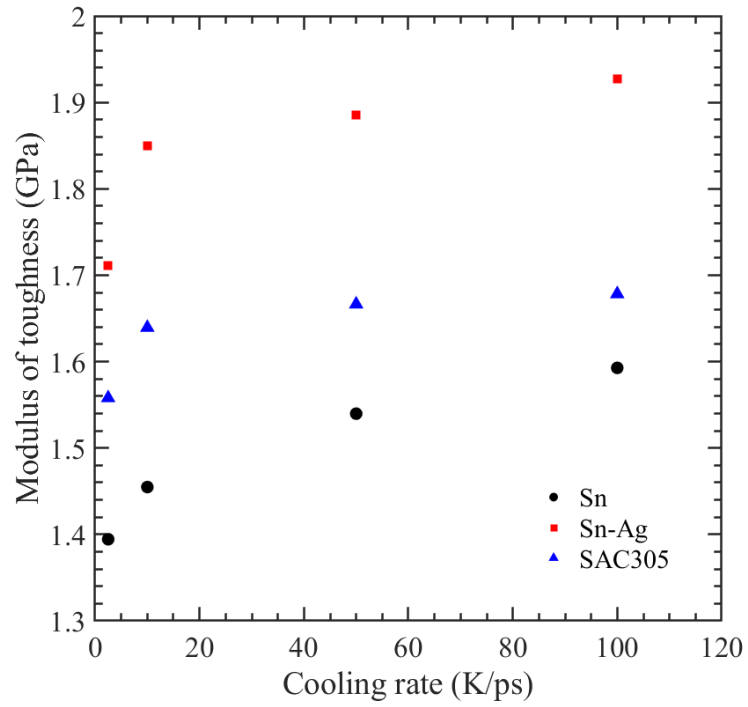


Figure 7: Variation of modulus of toughness with cooling rate

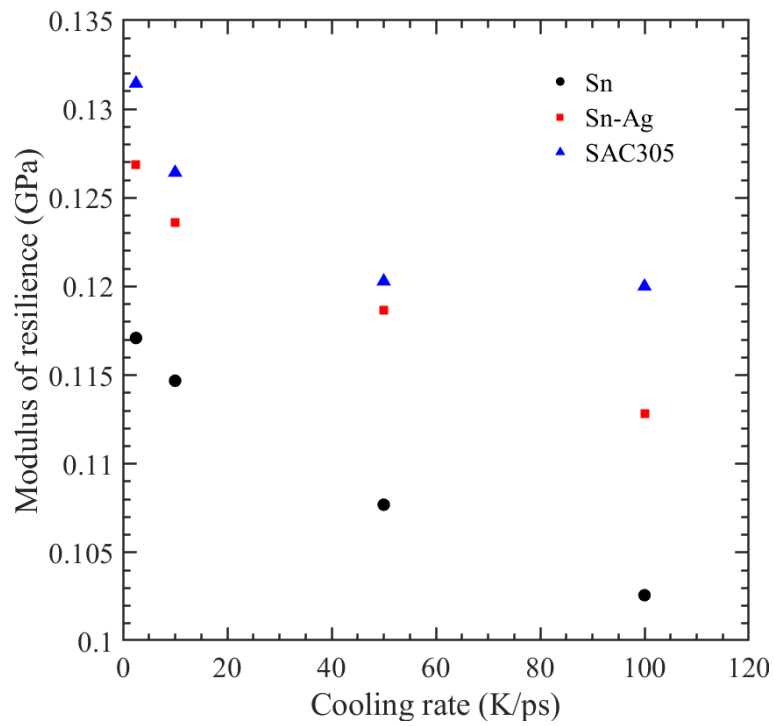


Figure 8: Variation of modulus of resilience with cooling rate

Figure 9 presents the relationship between the coefficient of thermal expansion (CTE) and cooling rates for all the materials. As the materials temperature is decreased under NPT, the simulation model size is also decreasing. The recorded size is used to calculate the CTE according to the Equation (4). The size that is used in the equation is calculated after the temperature reaches 200 °C. For all of the materials that were discussed, the value of CTE drops as the cooling rate is increased. At higher cooling rate, the atoms do not get enough time to contract which is a reason behind the decreasing trend of CTE. The CTE at 50 K/ps and 100 K/ps is not negligible like the properties discussed in the preceding section.

$$\alpha_v = \frac{1}{V} \frac{dV}{dT} \quad (4)$$

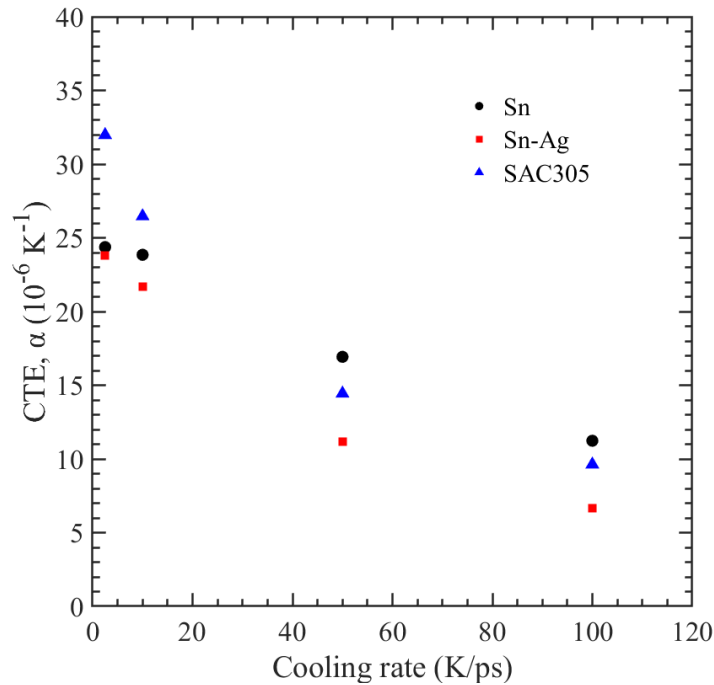


Figure 9: Variation of coefficient of thermal expansion (CTE) over different cooling rates

4.2 EFFECT OF EXPONENTIAL COOLING

When a material is air-cooled, water-cooled, and furnace-cooled, the temperature decays exponentially [60] rather than linearly. To present a similar situation, in this study, an exponential cooling is employed to all materials. The stress-strain behavior after the exponential cooling to room temperature is demonstrated in Figure 10 and the properties have been compared against the properties for 2.5 K/ps. The outcomes of the exponential cooling are closely similar to those of a cooling rate of 2.5 K/ps, with the former showing a slightly higher ultimate tensile strength. The

UTS, YM, modulus of toughness and modulus of resilience are presented in Table 3 for all materials.

Table 3: Data from tensile test of exponential cooling

Materials	UTS (GPa)	YM (GPa)	Modulus of toughness (GPa)	Modulus of resilience (GPa)
Sn	6.46	83.47	1.50	0.104
Sn-Ag	6.51	91.94	1.69	0.118
SAC305	6.91	108.64	1.62	0.120

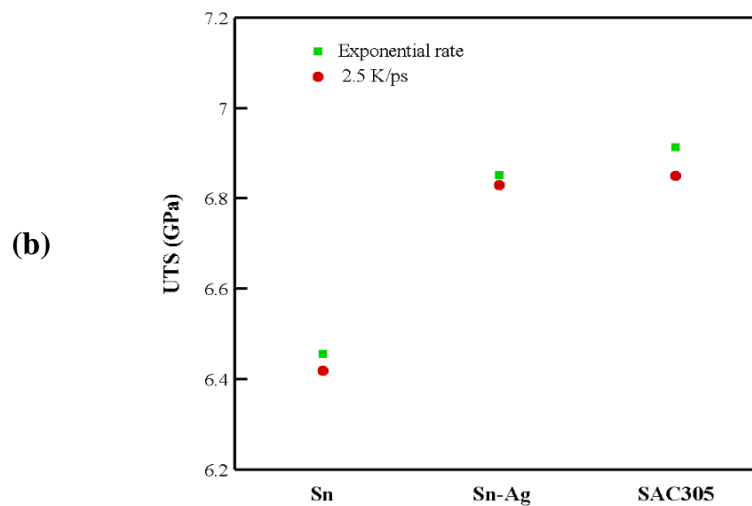
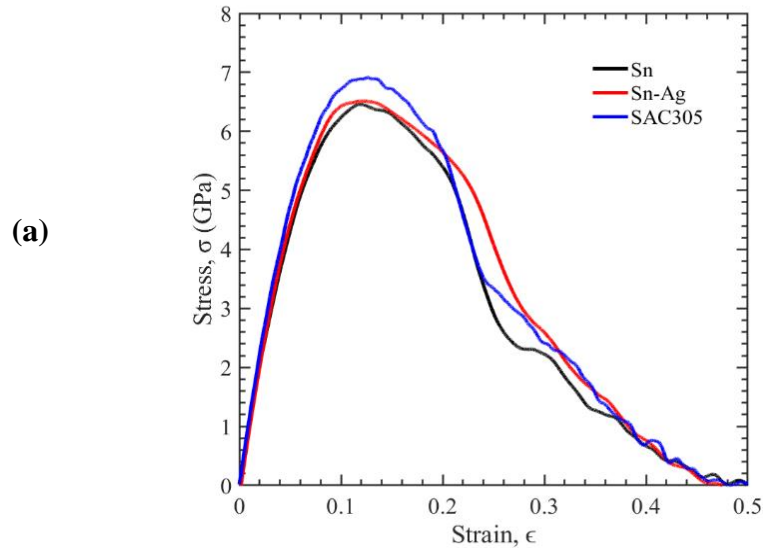


Figure 10: (a) Stress vs strain curve for different materials when cooled exponentially. (b) Differences in the UTS when cooled linearly (2.5 K/ps) and exponentially

4.3 EFFECTS OF CYCLIC LOADING

Figures 11, 12, and 13 illustrate the behavior of the stress-strain curve of Sn, Sn-Ag, and SAC305, respectively for all cooling rates under cyclic loading conditions. Sn, Sn-Ag, and SAC305 are subjected to -10% to 10% of their original length for 10 cycles at 2.5 K/ps, 10 K/ps, and 50 K/ps and 100 K/ps, respectively at 300 K. The 100 K/ps yields comparable results to the 50 K/ps, similar to the case in tensile test. Lead-free solder alloys deform elastically between 6-8% strain and plastic deformation occurs up to 10% strain. The loading direction is then reversed, signifying the beginning of compression. However, no elastic deformation is observed in the following cycles. This behavior is also supported by experiments conducted by Mustafa et al. [60].

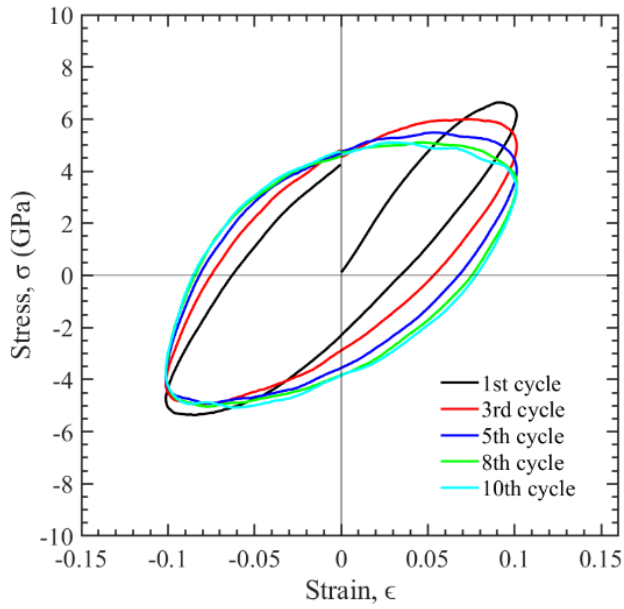
Figure 14 depicts the hysteresis loop area for the second, fifth, eighth, and tenth cycles of all cooling rates mentioned. The hysteresis loop area represents the amount of energy dissipated per cycle and is directly linked to the damage accumulated by the material during each loading-unloading cycle [61]. The variation in hysteresis loop areas is evident across all the cooling rates and the solder alloys. In subsequent cycles, however, the difference progressively diminishes. The areas for all cooling rates converge to a certain value, indicating that saturation is reached in a shorter number of cycles. This is due to redistribution of stresses within the materials. Another significant observation is that the area increases with each cycle. As the number of cycles increases, the area of damage also stabilizes. As the number of cycles increases, the material may experience cumulative degradation, such as fatigue or plastic deformation, which can cause the hysteresis loop area to increase. Figure 15 is plotted for the 2nd, 5th, and 10th cycles to better illustrate the variation in the area caused by the cooling rates of each material. The damage accumulation in SAC305 is the highest among all the materials and Sn being the lowest in 2nd cycle. But in the 5th and 10th cycles, the areas for Sn-Ag and SAC305 are similar.

The stress amplitude has been calculated using Equation (5) for lead-free solder materials. The stress amplitude parameter is commonly employed to anticipate the fatigue endurance of a given material. The fatigue life of the material is directly proportional to the stress amplitude, such that a decrease in stress amplitude results in an increase in the material's fatigue life. Figure 16

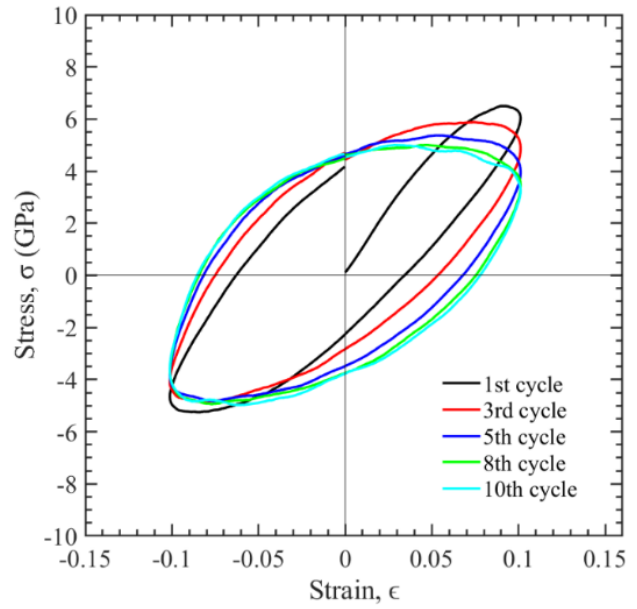
demonstrates how the stress amplitude evolves over time for different cooling speeds. The stress amplitude diminishes as the number of cycles increases. This is due to cyclic softening occurs with the number of cycles [62]. Under cyclic loading, plastic deformation, and the accumulation of plastic strain in subsequent cycles are mostly to blame for the cyclic softening that takes place with increasing numbers of cycles. Over the number of cycles, the stress amplitude in any given case of cooling rate begins to approach the point of saturation. The number of cycles required to attain the saturation level increases with lower cooling rates, such as 2.5 K/ps and 10 K/ps. Higher cooling rates, such as 50 K/ps and 100 K/ps, reach the saturation point in a shorter number of cycles.

$$\text{Stress Amplitude} = \frac{\sigma_{max} - \sigma_{min}}{2} \quad (5)$$

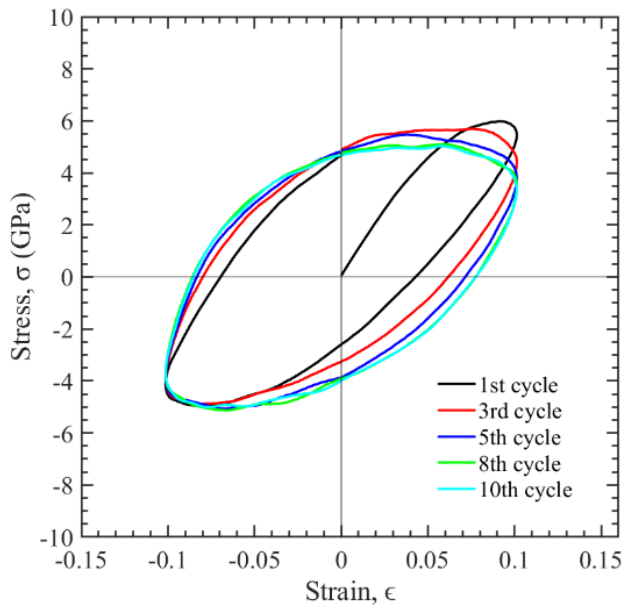
To elucidate the reason behind the loop converging to certain value, the radial distribution function (RDF) for Sn, Sn-Ag, and SAC305 at different cooling rates is shown in Figure 17 for 2nd and 10th cycle. RDF can be utilized for investigating structural changes within a material [63]. In the 2nd cycle, the probability of finding another particle at a particular distance is different for each cooling rate. But at the 10th cycle, the probability of finding another particle is nearly unchanged, suggesting that the interatomic distances between the atoms remain consistent. This indicates that the structural changes occurring within the system are relatively similar as the number of cycles increases.



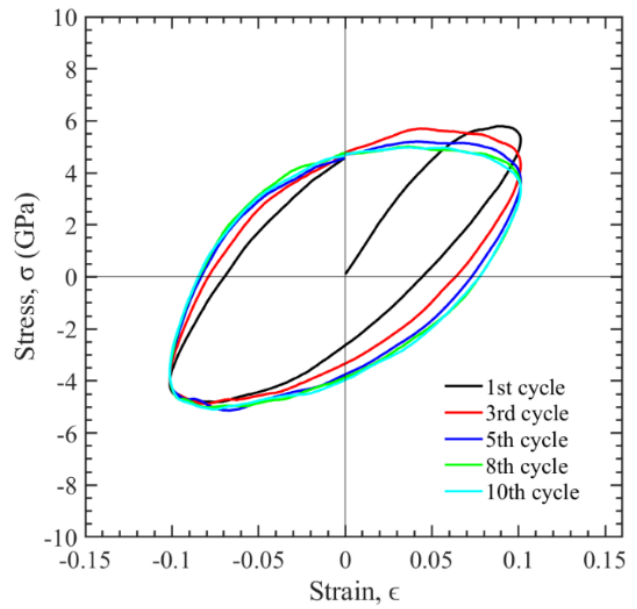
(a)



(b)

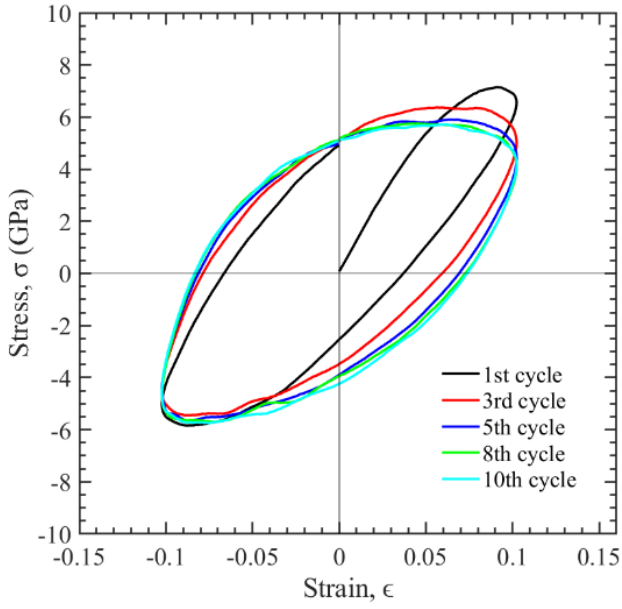


(c)

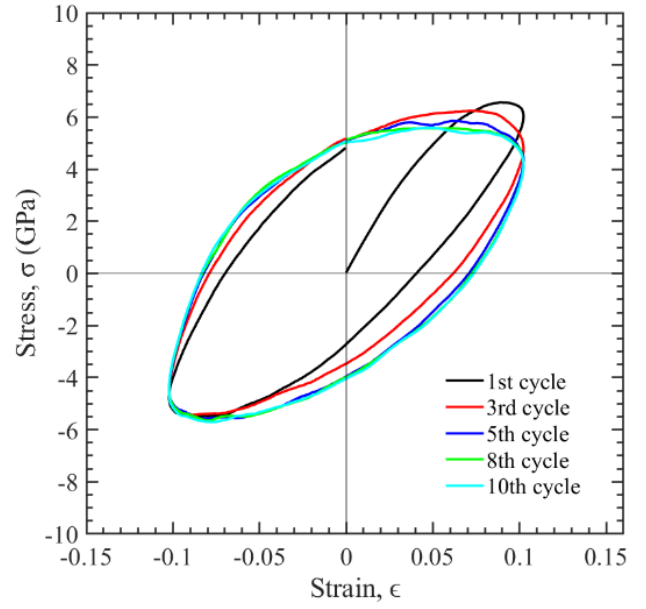


(d)

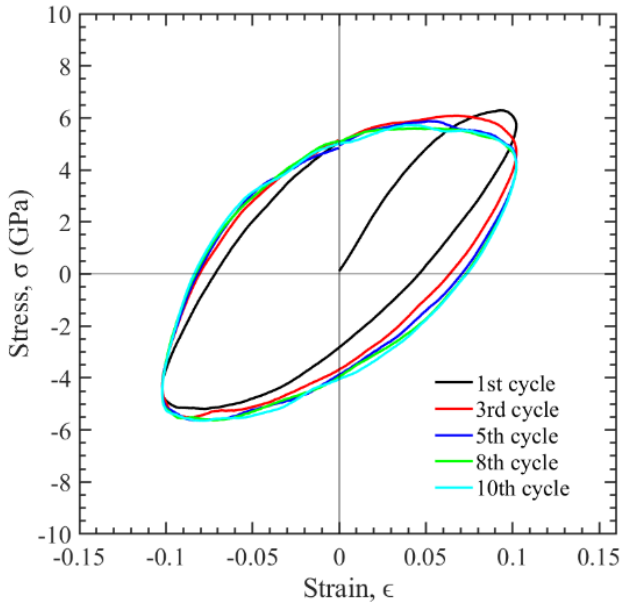
Figure 11: Stress vs strain curves for Sn during cyclic loading when cooled at (a) 2.5K/ps, (b) 10 K/ps, (c) 50 K/ps, and (d) 100 K/ps



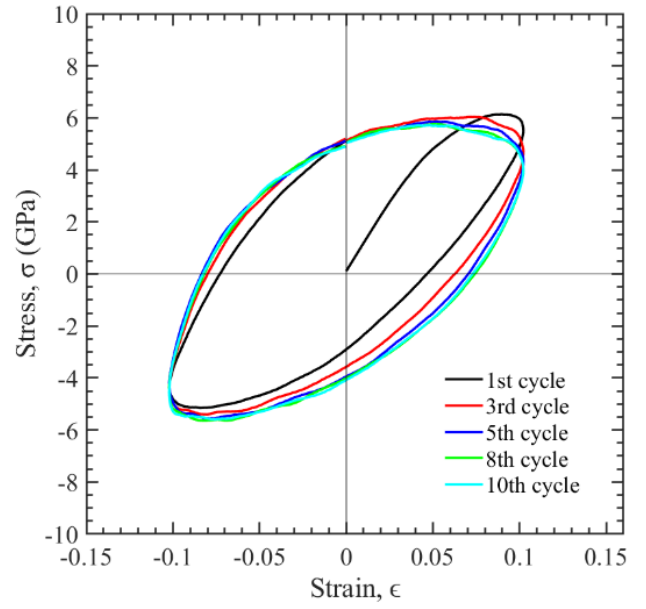
(a)



(b)

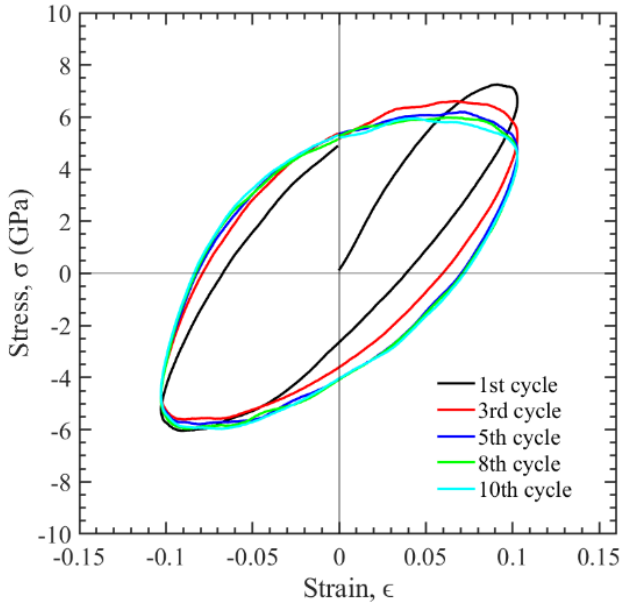


(c)

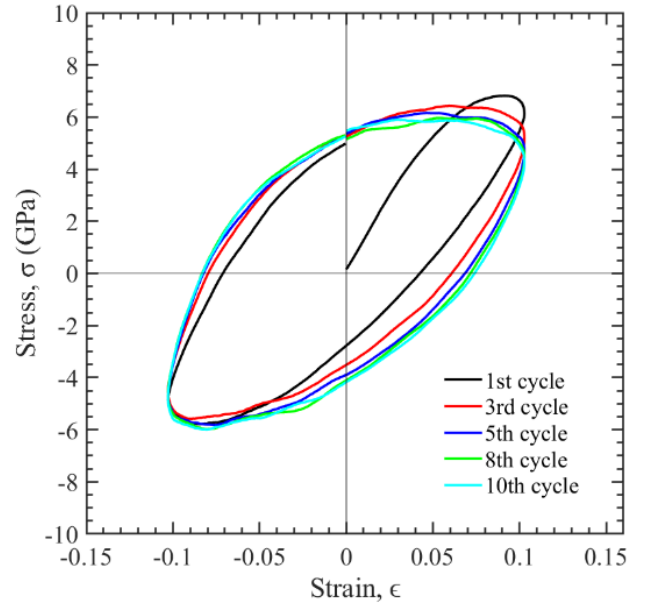


(d)

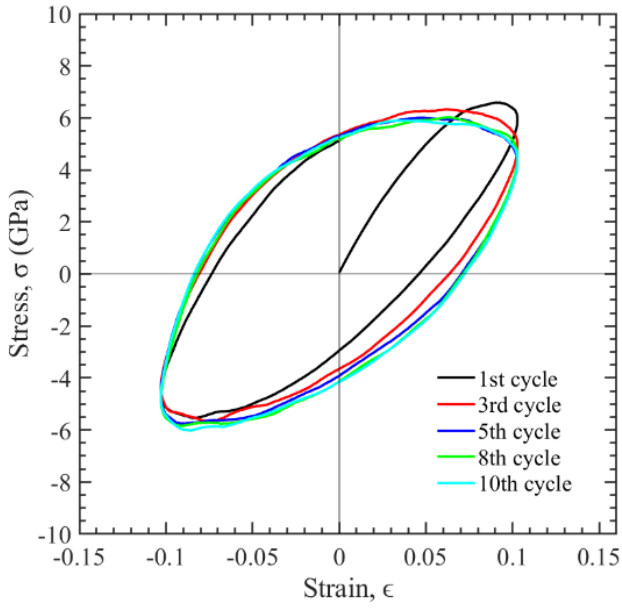
Figure 12: Stress vs strain curves for Sn-Ag during cyclic loading when cooled at (a) 2.5 K/ps, (b) 10 K/ps, (c) 50 K/ps, and (d) 100 K/ps



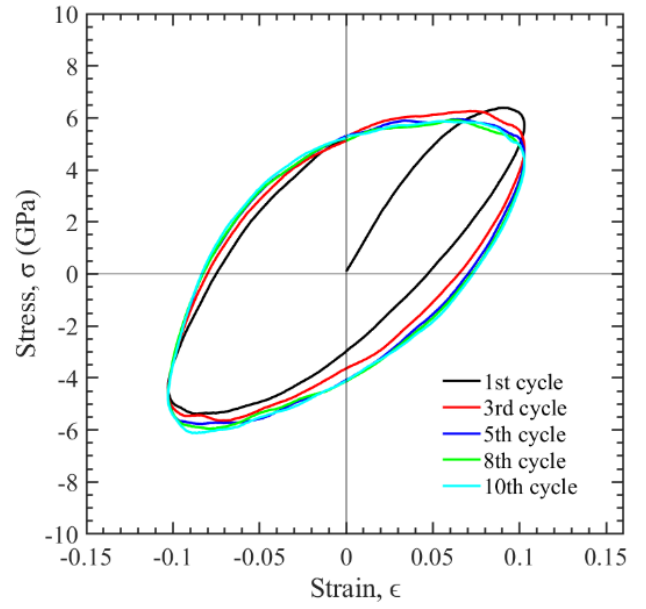
(a)



(b)



(c)



(d)

Figure 13: Stress vs strain curves for SAC305 during cyclic loading when cooled at (a) 2.5 K/ps, (b) 10 K/ps, (c) 50 K/ps, and (d) 100 K/ps

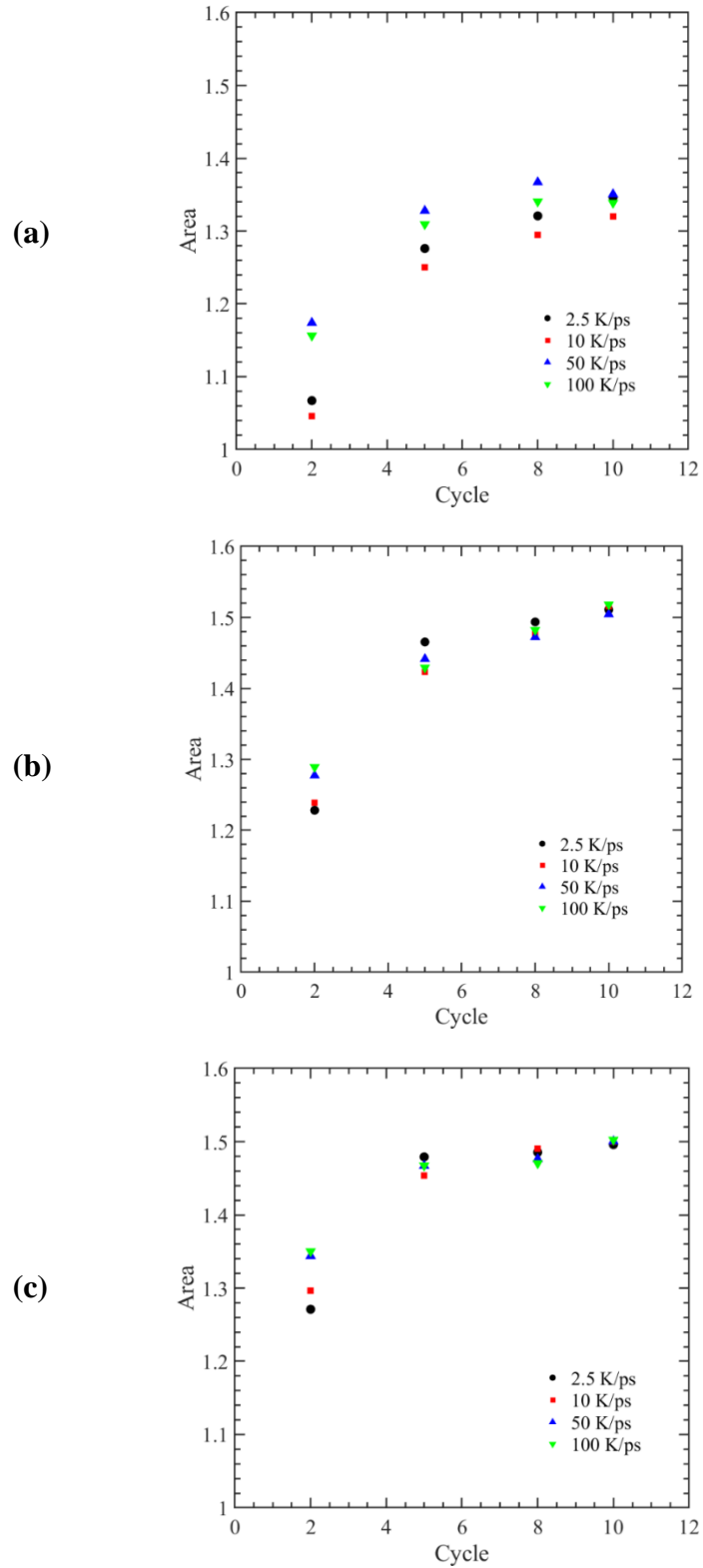


Figure 14: Variation of the area of hysteresis loop for different cooling rates of (a) Sn, (b) Sn-Ag, and (c) SAC305

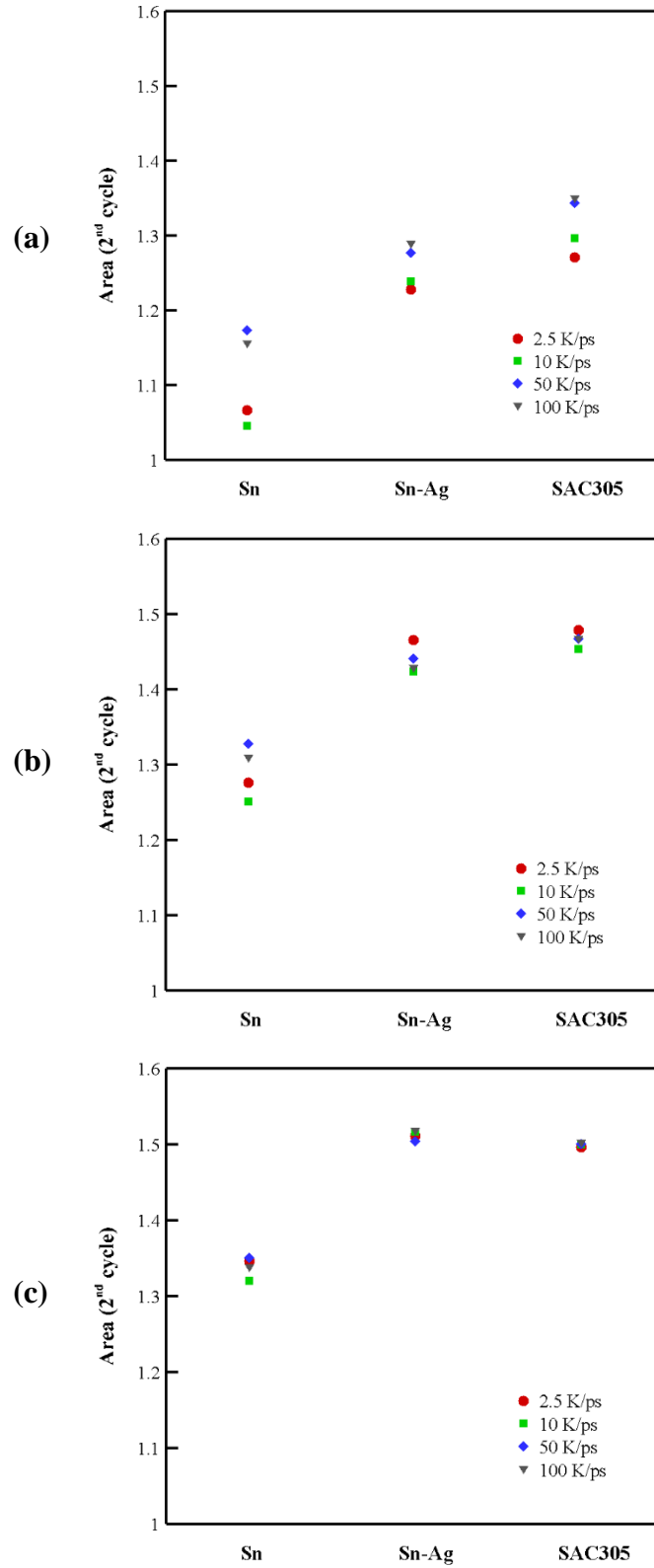


Figure 15: Comparison among the materials in terms of loop area at (a) 2nd, (b) 5th, and (c) 10th cycle

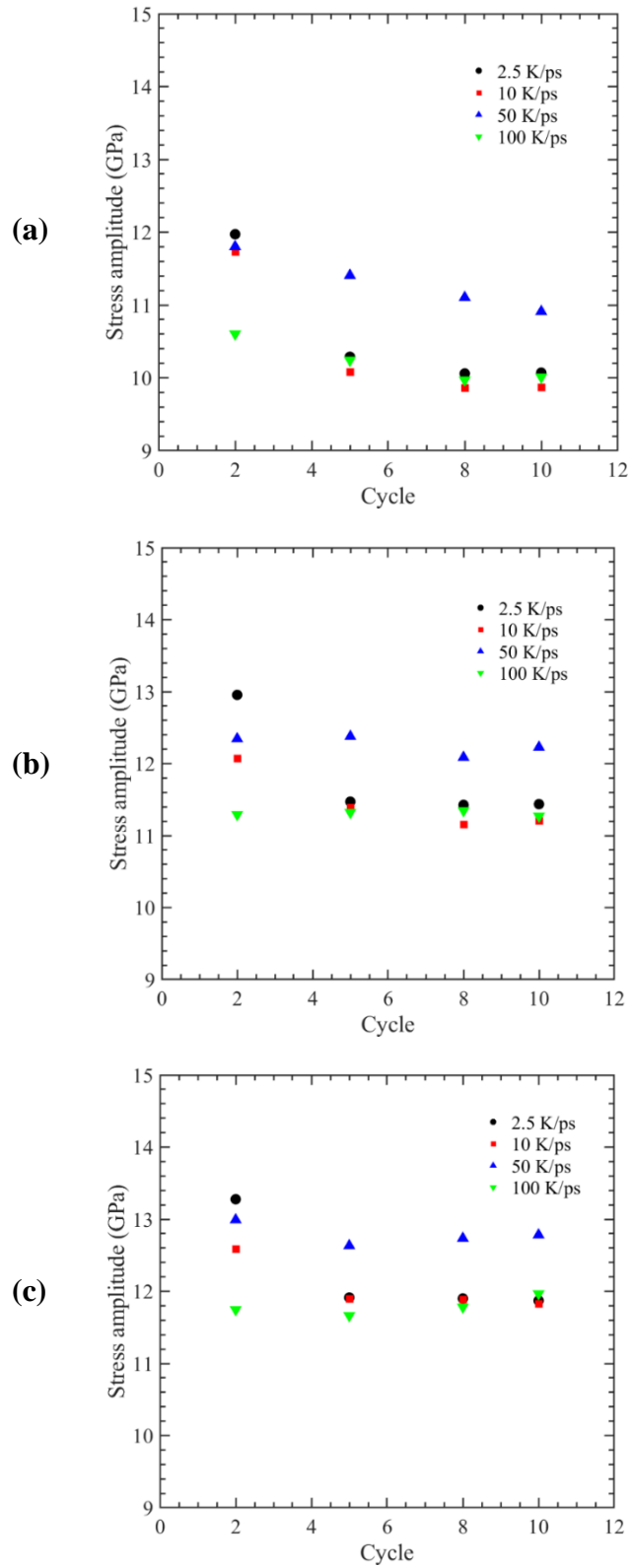


Figure 16: Variation of the stress amplitude for different cooling rates for (a) Sn, (b) Sn-Ag, and (c) SAC305

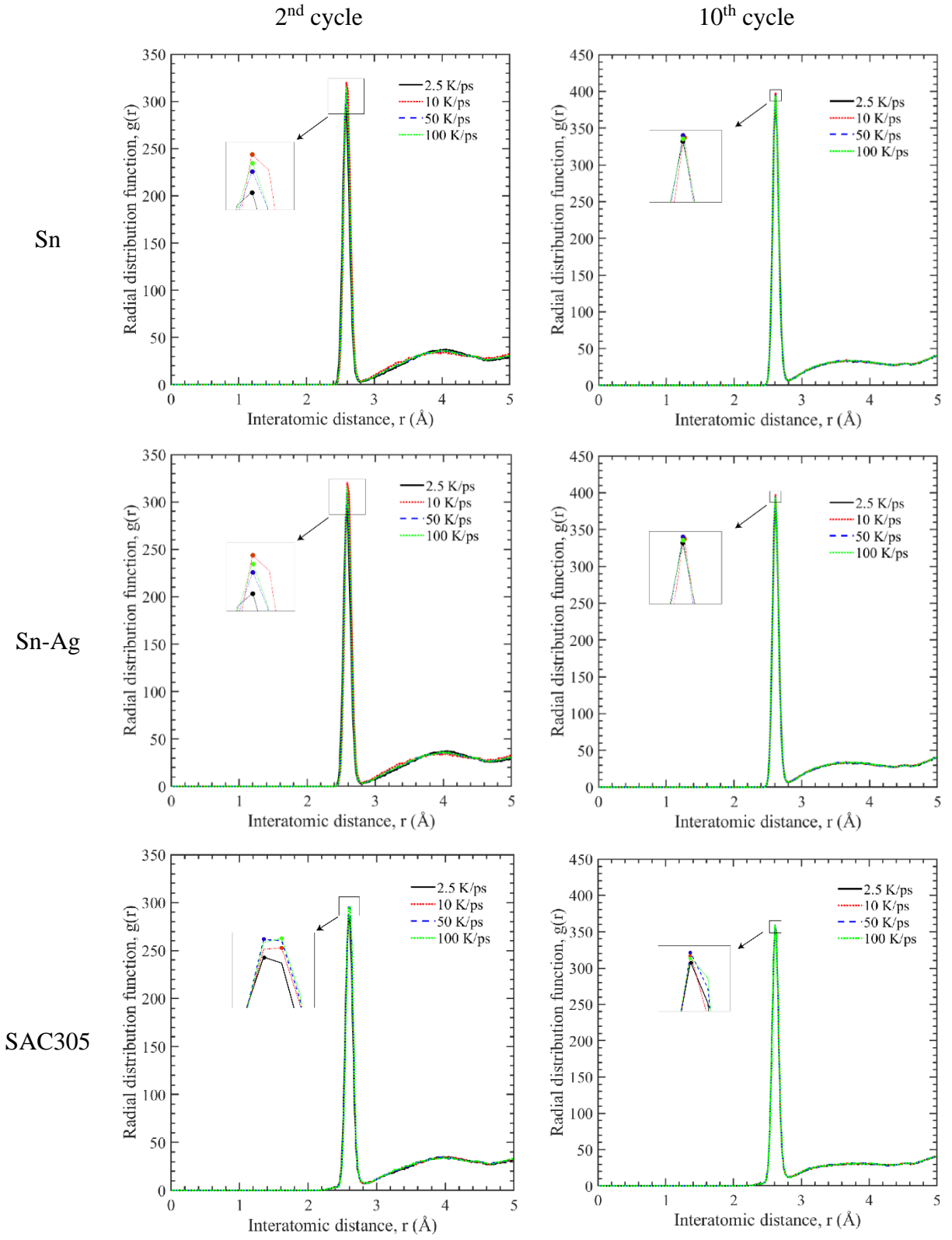


Figure 17: Variation of RDF for different cooling rates of Sn, Sn-Ag and SAC305 during 2nd cycle and 10th cycle

5. CONCLUSION

In this research, molecular dynamics is employed to model and simulate the changes in the mechanical and thermal characteristics of lead-free solder materials at the nanoscale. This investigation can offer valuable insights for enhancing solder joint quality and reliability in electronic assemblies, ensuring sound solidification, and mitigating potential defects. Atomistic simulations were conducted to explore the influence of cooling rates on materials subjected to both uniaxial tensile and cyclic loading. The findings indicate that-

- I. As the cooling rate rises, the ultimate tensile strength and Young's modulus consistently decline across all lead-free solder alloy cases, primarily due to an increase in the number of defects.
- II. With the increasing cooling rate from 2.5 K/ps to 100 K/ps, the modulus of toughness experiences an increasing trend, while the modulus of resilience exhibits a decreasing trend across all materials.
- III. Because solder alloys have less time to contract at higher cooling rates, their coefficient of thermal expansion decreases.
- IV. When cyclic loading is applied, damage accumulation increases with cycle in case of lead-free solders. Hysteresis loop areas of all lead-free solder materials converge at the 10th cycle indicating the stability in damage accumulation.
- V. Initially, during cyclic loading, there are variations in interatomic distances, but as the number of cycles increases, they eventually stabilize and stay consistent.

ACKNOWLEDGEMENT

We would like to express our sincere appreciation to the Bangladesh University of Engineering and Technology (BUET) for their exceptional support in providing a high-quality computer laboratory, which was instrumental in the successful completion of this research project.

REFERENCES

- [1] J. M. Davis, R. W. Elias, and L. Grant, "Current issues in human lead exposure and regulation of lead," *Neurotoxicology*, vol. 14, no. 2-3, pp. 15-27, 1993.

- [2] K. J. Puttlitz and K. A. Stalter, "Handbook of lead-free solder technology for microelectronic assemblies". *CRC Press*, 2004.
- [3] O. Salmela, "Acceleration factors for lead-free solder materials," *IEEE transactions on components and packaging technologies*, vol. 30, no. 4, pp. 700-707, 2007.
- [4] C. Wu, D. Q. Yu, C. Law, and L. Wang, "Properties of lead-free solder alloys with rare earth element additions," *Materials Science and Engineering: R: Reports*, vol. 44, no. 1, pp. 1-44, 2004.
- [5] H. R. Kotadia, P. D. Howes, and S. H. Mannan, "A review: On the development of low melting temperature Pb-free solders," *Microelectronics Reliability*, vol. 54, no. 6-7, pp. 1253-1273, 2014.
- [6] E. E. Mhd Noor, N. F. Mhd Nasir, and S. R. A. Idris, "A review: lead free solder and its wettability properties," *Soldering & Surface Mount Technology*, vol. 28, no. 3, pp. 125-132, 2016.
- [7] M. McCormack, S. Jin, G. Kammlott, and H. Chen, "New Pb-free solder alloy with superior mechanical properties," *Applied Physics Letters*, vol. 63, no. 1, pp. 15-17, 1993.
- [8] A. Schubert, H. Walter, R. Dudek, B. Michel, G. Lefranc, J. Otto, and G. Mitic , "Thermo-mechanical properties and creep deformation of lead-containing and lead-free solders," *Proceedings International Symposium on Advanced Packaging Materials Processes, Properties and Interfaces*, pp. 129-134, 2001.
- [9] K. Suganuma, "Lead-free soldering in electronics: Science, technology, and environmental impact". *CRC Press*, 2003.
- [10] J. Glazer, "Microstructure and mechanical properties of Pb-free solder alloys for low-cost electronic assembly: a review," *Journal of Electronic Materials*, vol. 23, pp. 693-700, 1994.
- [11] Y. Li, K.-s. Moon, and C. Wong, "Electronics without lead," *Science*, vol. 308, no. 5727, pp. 1419-1420, 2005.
- [12] M. Abteu and G. Selvaduray, "Lead-free Solders in Microelectronics," *Materials Science and Engineering: R: Reports*, vol. 27, no. 5, pp. 95-141, 2000.
- [13] S. Cheng, C.-M. Huang, and M. Pecht, "A review of lead-free solders for electronics applications," *Microelectronics Reliability*, vol. 75, pp. 77-95, 2017.

- [14] S. K. Kang, P. Lauro, D. Y. Shih, D. W. Henderson, and K. J. Puttlitz, "Microstructure and mechanical properties of lead-free solders and solder joints used in microelectronic applications," *IBM Journal of Research and Development*, vol. 49, no. 4.5, pp. 607-620, 2005.
- [15] M. Abtew and G. Selvaduray, "Lead-free solders in microelectronics," *Materials Science and Engineering: R: Reports*, vol. 27, no. 5-6, pp. 95-141, 2000.
- [16] A. Kroupa *et al.*, "Current problems and possible solutions in high-temperature lead-free soldering," *Journal of Materials Engineering and Performance*, vol. 21, pp. 629-637, 2012.
- [17] D. Suraski and K. Seelig, "The current status of lead-free solder alloys," *IEEE Transactions on Electronics Packaging Manufacturing*, vol. 24, no. 4, pp. 244-248, 2001.
- [18] O. R. Adetunji, R. A. Ashimolowo, P. O. Aiyedun, O. M. Adesusi, H. O. Adeyemi, and O. R. Oloyede, "Tensile, hardness and microstructural properties of Sn-Pb solder alloys," *Materials Today: Proceedings*, vol. 44, pp. 321-325, 2021.
- [19] I. Shohji, T. Yoshida, T. Takahashi, and S. Hioki, "Tensile properties of Sn-Ag based lead-free solders and strain rate sensitivity," *Materials Science and Engineering: A*, vol. 366, no. 1, pp. 50-55, 2004.
- [20] M.-L. Wu and J.-S. Lan, "Reliability and failure analysis of SAC 105 and SAC 1205N lead-free solder alloys during drop test events," *Microelectronics Reliability*, vol. 80, pp. 213-222, 2018.
- [21] H. L. J. Pang, Y. P. Wang, X. Q. Shi, and Z. P. Wang, "Sensitivity study of temperature and strain rate dependent properties on solder joint fatigue life," in *Proceedings of 2nd Electronics Packaging Technology Conference (Cat. No.98EX235)*, 1998, pp. 184-189.
- [22] P. Lall, V. Yadav, J. Suhling, and D. Locker, "Low Temperature Material Characterization of Lead-Free SAC Solder Alloy at High Strain Rate After Prolonged High Temperature Storage," in *ASME 2021 International Technical Conference and Exhibition on Packaging and Integration of Electronic and Photonic Microsystems*, pp. V001T07A021, 2021.
- [23] M. R. Chowdhury, S. Ahmed, A. Fahim, J. C. Suhling and P. Lall, "Mechanical characterization of doped SAC solder materials at high temperature," *2016 15th IEEE Intersociety Conference on Thermal and Thermomechanical Phenomena in Electronic Systems (ITherm)*, Las Vegas, NV, USA, pp. 1202-1208, 2016.

- [24] C. Basaran, A. Cartwright, and Y. Zhao, "Experimental Damage Mechanics of Microelectronics Solder Joints under Concurrent Vibration and Thermal Loading," *International Journal of Damage Mechanics*, vol. 10, no. 2, pp. 153-170, 2001.
- [25] S. Wiese and S. Rzepka, "Time-independent elastic–plastic behaviour of solder materials," *Microelectronics Reliability*, vol. 44, no. 12, pp. 1893-1900, 2004.
- [26] A. Schubertt, R. Dudek, E. Auerswald, A. Gollbardt, B. Michel, and H. Reichl, "Fatigue life models for SnAgCu and SnPb solder joints evaluated by experiments and simulation," *Electronic components and technology conference*, pp. 603-610, 2003.
- [27] M. Motalab, R. Paul, S. Saha, S. Mojumder, M. Ahmed, and J. Suhling, "Atomistic analysis of the thermomechanical properties of Sn–Ag–Cu solder materials at the nanoscale with the MEAM potential," *Journal of Molecular Modeling*, vol. 25, pp. 1-10, 2019.
- [28] L. Zhang, D. Xiong, J. Li, L. Yin, Z. Yao, G. Wang, L. Zhang, and H. Zhang., "Molecular dynamics simulation of the interfacial evolution and whisker growth of copper-tin coating under electrothermal coupling," *Computational Materials Science*, vol. 202, p. 110981, 2022.
- [29] J. Zhang, J. Yang, L. Liang, Y. Xu, and J. Guo, "A molecular dynamics investigation of the micro-mechanism for vacancy formation between Ag_3Sn and βSn under electromigration," *Molecular Physics*, vol. 116, no. 1, pp. 99-106, 2018.
- [30] Y. Li, L. Xu, L. Zhao, K. Hao, and Y. Han, "Shear deformation behavior and failure mechanisms of graphene reinforced Sn-based solder joints bonded by transient current," *Materials & Design*, vol. 224, p. 111369, 2022.
- [31] B. Chen, W.-P. Wu, M.-X. Chen, and Y.-F. Guo, "Molecular dynamics study of fatigue mechanical properties and microstructural evolution of Ni-based single crystal superalloys under cyclic loading," *Computational Materials Science*, vol. 185, p. 109954, 2020.
- [32] S. M. A. A. Alvi, A. Faiyad, M. A. M. Munshi, M. Motalab, M. M. Islam, and S. Saha, "Cyclic and tensile deformations of Gold–Silver core shell systems using newly parameterized MEAM potential," *Mechanics of Materials*, vol. 169, p. 104304, 2022.
- [33] H. G. Nguyen, T. H. Fang, and D. Q. Doan, "Cyclic plasticity and deformation mechanism of AlCrCuFeNi high entropy alloy," *Journal of Alloys and Compounds*, vol. 940, p. 168838, 2023/04/15/ 2023.

- [34] G. S. Grest, D. J. Srolovitz, and M. P. Anderson, "Computer simulation of grain growth—IV. Anisotropic grain boundary energies," *Acta Metallurgica*, vol. 33, no. 3, pp. 509-520, 1985.
- [35] R. W. Lewis and P. M. Roberts, "Finite element simulation of solidification problems," in *Modelling the Flow and Solidification of Metals*, T. J. Smith Ed. Dordrecht: Springer Netherlands, pp. 61-92, 1987.
- [36] E. Miyoshi and T. Takaki, "Extended higher-order multi-phase-field model for three-dimensional anisotropic-grain-growth simulations," *Computational Materials Science*, vol. 120, pp. 77-83, 2016.
- [37] A. J. Haslam, S. R. Phillpot, D. Wolf, D. Moldovan, and H. Gleiter, "Mechanisms of grain growth in nanocrystalline fcc metals by molecular-dynamics simulation," *Materials Science and Engineering: A*, vol. 318, no. 1, pp. 293-312, 2001.
- [38] Y. Shibuta, S. Sakane, E. Miyoshi, S. Okita, T. Takaki, and M. Ohno, "Heterogeneity in homogeneous nucleation from billion-atom molecular dynamics simulation of solidification of pure metal," *Nature Communications*, vol. 8, no. 1, p. 10, 2017.
- [39] J. W. Elmer, S. M. Allen, and T. W. Eagar, "Microstructural development during solidification of stainless steel alloys," *Metallurgical Transactions A*, vol. 20, no. 10, pp. 2117-2131, 1989.
- [40] A. Mahata, M. A. Zaeem, and M. I. Baskes, "Understanding homogeneous nucleation in solidification of aluminum by molecular dynamics simulations," *Modelling and Simulation in Materials Science and Engineering*, vol. 26, no. 2, p. 025007, 2018.
- [41] J. Li *et al.*, "Tuning the mechanical behavior of high-entropy alloys via controlling cooling rates," *Materials Science and Engineering: A*, vol. 760, pp. 359-365, 2019.
- [42] B. Shen, C.Y. Liu, Y. Jia, G.Q. Yue, F.S. Ke, H.B. Zhao, L.Y. Chen, S.Y. Wang, C.Z. Wang, and K.M. Ho, "Molecular dynamics simulation studies of structural and dynamical properties of rapidly quenched Al," *Journal of Non-Crystalline Solids*, vol. 383, pp. 13-20, 2014.
- [43] S. Li, S. Cui, H. Chen, J. Li, H. Huang, and H. Luo, "Effect of cooling rates on solidification, microstructure and mechanical properties in tungsten," *CrystEngComm*, vol. 21, no. 26, pp. 3930-3938, 2019.

- [44] T. Shu, N. Hu, F. Liu, and G. J. Cheng, "Nanoparticles induced intragranular and dislocation substructures in powder bed fusion for strengthening of high-entropy-alloy," *Materials Science and Engineering: A*, vol. 878, p. 145110, 2023.
- [45] M. I. Baskes, "Modified embedded-atom potentials for cubic materials and impurities," *Physical Review B*, vol. 46, no. 5, pp. 2727-2742, 1992.
- [46] M. I. Baskes, J. S. Nelson, and A. F. Wright, "Semiempirical modified embedded-atom potentials for silicon and germanium," *Physical Review B*, vol. 40, no. 9, pp. 6085-6100, 1989.
- [47] H. Fei, K. Yazzie, J. Williams, and H. Jiang, "Multiscale Modeling of the Interfacial Fracture Behavior in the Sn-Cu₆ Sn₅-Cu System," *Journal of Computational and Theoretical Nanoscience*, vol. 8, pp. 873-880, 2011.
- [48] H. Dong, L. Fan, K.S. Moon, C. P. Wong, and M. Baskes, "MEAM molecular dynamics study of lead free solder for electronic packaging applications," *Modelling and Simulation in Materials Science and Engineering*, vol. 13, p. 1279, 2005.
- [49] R. Ravelo and M. Baskes, "Equilibrium and Thermodynamic Properties of Grey, White, and Liquid Tin," *Physical Review Letters*, vol. 79, no. 13, pp. 2482-2485, 1997.
- [50] S. Plimpton, "Fast Parallel Algorithms for Short-Range Molecular Dynamics," *Journal of Computational Physics*, vol. 117, no. 1, pp. 1-19, 1995.
- [51] A. Stukowski, "Visualization and analysis of atomistic simulation data with OVITO—the Open Visualization Tool," *Modelling and Simulation in Materials Science and Engineering*, vol. 18, no. 1, p. 015012, 2010.
- [52] M. Mustafa, Z. Cai, J. C. Suhling, and P. Lall, "The effects of aging on the cyclic stress-strain behavior and hysteresis loop evolution of lead free solders," in *2011 IEEE 61st Electronic Components and Technology Conference (ECTC)*, pp. 927-939, 2011.
- [53] M. Zhou, "A new look at the atomic level virial stress: on continuum-molecular system equivalence," *Proceedings of the Royal Society of London. Series A: Mathematical, Physical and Engineering Sciences*, vol. 459, no. 2037, pp. 2347-2392, 2003.
- [54] E. George, D. Das, M. Osterman, and M. Pecht, "Thermal Cycling Reliability of Lead-Free Solders (SAC305 and Sn3.5Ag) for High-Temperature Applications," *IEEE Transactions on Device and Materials Reliability*, vol. 11, no. 2, pp. 328-338, 2011.

- [55] E. V. Vernon and S. Weintraub, "The Measurement of the Thermal Expansion of Single Crystals of Indium and Tin with a Photoelectric Recording Dilatometer," *Proceedings of the Physical Society. Section B*, vol. 66, no. 10, p. 887, 1953.
- [56] A. Schubert, H. Walter, R. Dudek, B. Michel, G. Lefranc, J. Otto, and G Mitic , "Thermo-mechanical properties and creep deformation of lead-containing and lead-free solders," *Proceedings International Symposium on Advanced Packaging Materials Processes, Properties and Interfaces (IEEE Cat. No.01TH8562)*, pp. 129-134, 2001.
- [57] F. X. Che, E. C. Poh, W. H. Zhu, and B. S. Xiong, "Ag Content Effect on Mechanical Properties of Sn-xAg-0.5Cu Solders," in *2007 9th Electronics Packaging Technology Conference*, pp. 713-718, 2007.
- [58] K. Newman, "BGA brittle fracture - alternative solder joint integrity test methods," *Proceedings Electronic Components and Technology*, pp. 1194-1201 Vol. 2, 2005.
- [59] F. Song, S. W. R. Lee, K. Newman, B. Sykes, and S. Clark, "Brittle Failure Mechanism of SnAgCu and SnPb Solder Balls during High Speed Ball Shear and Cold Ball Pull Tests," *Proceedings 57th Electronic Components and Technology Conference*, 29, pp. 364-372, 2007.
- [60] M. Mustafa, Z. Cai, J. Suhling, and P. Lall, "The effects of aging on the cyclic stress-strain behavior and hysteresis loop evolution of lead free solders," *Proceedings - Electronic Components and Technology Conference*, pp. 927-939, 2011.
- [61] T. L. Jesse and L. M. David, "Degradation of an Ni-Ti alloy during cyclic loading," in *Proc.SPIE*, vol. 2189, pp. 326-341, 1994.
- [62] G. Kang and Y. Liu, "Uniaxial ratchetting and low-cycle fatigue failure of the steel with cyclic stabilizing or softening feature," *Materials Science and Engineering: A*, vol. 472, no. 1, pp. 258-268, 2008.
- [63] D. Srolovitz, T. Egami, and V. Vitek, "Radial distribution function and structural relaxation in amorphous solids," *Physical Review B*, vol. 24, no. 12, pp. 6936-6944, 1981.